

Spectral Energy Centroid: a Metric for Improving Performance and Analyzing Spectral Bias in Implicit Neural Representations

Tomasz Dądela*
Jagiellonian University
Kraków, Poland

Adam Kania*
GSK.ai
Baar, Switzerland

Maciej Rut*
Jagiellonian University
Kraków, Poland

Przemysław Spurek
Jagiellonian University
IDEAS
Kraków, Poland

Abstract

Implicit Neural Representations (INRs) model continuous signals using multilayer perceptrons (MLPs), enabling compact, differentiable, and high-fidelity representations of data across diverse domains. However, due to the low-frequency bias of MLPs that prevents effective learning of small details, the model’s frequency must be carefully tuned through the embedding layer. Prior work established that this tuning can be performed before training based on the target signal, but it did not account for the significant effect of model depth, indicating that our understanding of the relationship between frequency and INR performance remains limited. To gain insights into this relationship, we utilize the Spectral Energy Centroid (SEC) metric that quantifies the frequency of target images and the spectral bias of INR models. We show that SEC is a versatile tool for INR analysis, demonstrating its utility across three tasks: (1) a data-driven strategy (SEC-Conf) for hyperparameter selection that outperforms existing heuristics and is robust to model depth, (2) a reliable proxy for signal complexity, and (3) effective alignment of spectral biases across diverse INR architectures.

Implicit Neural Representations (INRs) have become a vital tool for scene modeling, robotics, and generative tasks [21], representing signals as continuous functions parameterized by MLPs. However, standard MLPs suffer from a low-frequency bias, making it difficult to capture fine details [22, 13]. To address this, architectures like *Siren* [17], *Fourier* [19], and *Finer* [6] introduce architectural inductive biases that facilitate the learning of fine details, in particular through a high-frequency input mapping controlled by an embedding frequency parameter.

However, in practice, selecting optimal embedding frequency parameter values is computationally expensive. Optimal settings vary significantly across target images [3], forcing practitioners to resort to costly hyperparameter sweeps or to rely on default values from original publications. This challenge is compounded in architectures like *Finer* or *Wire*



Figure 1: Visual comparison of performance of a large (4-layer) *Fourier* model after 1000 steps. The left block shows crops of the full image (right) for the default configuration of embedding frequency, and ones selected by FreSh and SEC-conf (SEC-conf is an example application of SEC). Leveraging Energy centroids (SEC), we achieve improved performance, with SEC-conf resulting in the sharpest image.

*Equal contribution.

[16], where multiple frequency-related hyperparameters jointly influence performance, making it difficult to know which ones to tune.

The FreSh [3] method represents the first attempt to mitigate this issue and simplify embedding frequency parameter selection for INR models by aligning the frequency of the model with the target image. FreSh assumes that for optimal learning, frequencies present in the image and the untrained model should be the same and aligns them by selecting an embedding frequency parameter that minimizes Wasserstein distance. This approach, while effective in certain settings, does not generalize to some particularly high-frequency models such as *Wire* and degrades in performance when model depth is modified. This degradation suggests a flaw in the assumption made by FreSh regarding the alignment of model and target signal frequencies. Based on our experiments, the relationship between the frequencies of the target signal and the model is not direct, but can be learned from data.

In this work, we investigate the spectral bias of INRs and its impact on performance across different target signals. To quantify the frequency content of target images and the spectral bias of INR models, we utilize the Spectral Energy Centroid metric (SEC). **We show that SEC is a general-purpose tool for INR spectral analysis, demonstrating its utility across three tasks.** We demonstrate that model architecture influences spectral bias, a dependency that undermines existing heuristics like FreSh which doesn't have a mechanism to account for model size. To address this, we propose a robust, data-driven strategy for embedding layer configuration (SEC-conf) that effectively handles varying model sizes, as shown in fig. 1. Furthermore, we provide a framework for aligning spectral biases across diverse architectures, demonstrating that such alignment can enable older models to match the performance of newer ones in specific settings. Finally, we validate SEC as a reliable proxy for signal complexity. Our main contributions are as follows:

- We utilize SEC to quantify the frequency of images and the spectral bias of INR models, revealing a strong dependency between model depth and spectral bias.
- We propose a data-driven strategy for hyperparameter selection (called SEC-conf) and alignment of spectral bias across architectures, outperforming existing heuristics.
- We demonstrate that SEC serves as a reliable proxy for signal complexity, strongly correlating with reconstruction quality.

1 Related works

Spectral bias refers to the tendency of neural networks to learn low-frequency components of a signal more rapidly than high-frequency ones [22, 13, 15, 2]. This phenomenon has been observed not only in MLPs but also in more complex architectures, such as diffusion models [20]. Spectral bias is often cited as one explanation for the generalization ability of neural networks [15]. However, it poses a significant challenge for INRs, as it suppresses high-frequency signals.

Implicit Neural Representations (INRs) represent signals - ranging from images and videos [7] to 3D scenes [8] and tabular data [10] - as continuous functions parameterized by MLPs. In this study, we focus on INRs for image representation, as their moderate computational requirements enable us to conduct a large-scale benchmark across diverse architectures and configurations. INRs learn a mapping from spatial or temporal coordinates to signal values (e.g., color or density). Unlike in standard learning scenarios, INR training involves dense supervision (e.g., every pixel in an image) with the explicit goal of high-fidelity signal reconstruction. In this overfitting regime, spectral bias becomes a critical bottleneck, hindering the capture of fine details and removing it to enable learning of a broad range of frequencies is a central focus in INR research [17, 19, 16, 6, 3]. This can be partially achieved through deeper models, as it was theoretically shown depth expands the set of representable frequencies, though with diminishing magnitude for higher harmonics [23]. However, many state-of-the-art approaches primarily solve this issue with a high-frequency embedding in the input layer, governed by a hyperparameter we refer to as the *embedding frequency parameter*.

Siren [17] is one of the earliest and most influential INR architectures. It employs sinusoidal activations throughout the network, enabling it to represent high-frequency signals effectively. Its first layer applies a scaled sinusoidal mapping, $\sin(\omega_s W \mathbf{x} + \mathbf{b})$, where ω_s serves as the primary frequency parameter controlling the network's bandwidth². Although all layers use sine activations, mainly the first layer affects the frequency bias, as later layers use relatively small scales.

²We deviate from the original notation to avoid collisions between *Siren*, *Finer*, and *Wire*.

Fourier features [19] utilize a fixed high-frequency embedding of the input coordinates, typically followed by an MLP with ReLU activations. The embedding utilizes frequencies sampled from a Gaussian distribution, where the standard deviation σ directly controls the spectral bias (see eq. (7)).

Wire [16] employs a continuous complex Gabor wavelet as its activation, which is governed by two hyperparameters: the frequency parameter ω_w and a spatial compactness parameter s_0 . Unlike in *Siren* or *Fourier*, this activation is re-used at every layer without any change to its parameters, leading to a significant frequency increase throughout the model (see fig. 5 and eq. (8)). In this work, we focus on ω_w as the relevant embedding frequency parameter, while fixing $s_0 = 10$ across all experiments.

Finer [6] employs a variable-periodic activation function whose frequency increases with the distance from the origin. These activations are governed by two parameters that jointly influence the frequency behavior, making the model more challenging to tune in practice. Specifically, *Finer* introduces a *Siren*-like frequency parameter ω_f together with an additive bias term (see eq. (9)).

Initialization and configuration strategies address spectral bias through specialized weight initialization, meta-learning, or automated hyperparameter selection. Meta-learning methods [14, 18] learn initializations that facilitate rapid convergence, though they entail significant computational overhead. Recent efficient initialization schemes, such as FreSh, TUNER [9], and WINNER [1], provide alternatives that avoid this pre-training cost. However, TUNER and WINNER are restricted in their applicability, as they are compatible only with *Siren*. FreSh [3] automates the selection of frequency parameters for INRs. Operating on the premise that the spectral bias of an untrained network is characterized by the frequency spectrum of its output at initialization, FreSh selects hyperparameters by minimizing the Wasserstein distance between the spectrum of the initialized model’s output and that of the target signal. Although effective in many scenarios, we demonstrate that this heuristic overlooks the influence of model depth and width on spectral bias, often resulting in suboptimal configurations for non-standard model sizes. Additionally, the full frequency spectrum is ill-suited for further analysis due to its multidimensional nature, making its applications limited.

2 Motivation

Implicit Neural Representations require careful tuning of the embedding frequency parameter to capture high-frequency components of a signal. While previous work has established that the optimal embedding configuration is highly dependent on the target image [3], the influence of the network architecture itself remains under-explored, as we show in this section.

We conduct a controlled experiment using models of varying sizes: small (S, 2×128), medium (M, 3×256), and large (L, 4×512). For each configuration, we perform a dense grid search over frequency parameters, training on a diverse set of 90 images. The grid search is described in more detail in section 4. We report the best performing configurations across several architectures in fig. 2, along with those selected by FreSh and SEC-conf. We observe that the optimal value of embedding frequency systematically increases with model size, indicating that the network’s capacity to utilize high-frequency input signals increases with its size. This dependency poses a challenge for FreSh [3], which fails to adapt to this architectural shift and doesn’t follow the oracle. Specifically, while the optimal parameter values increase with model size, the embedding frequencies selected by FreSh decrease or remain relatively constant. This results in frequency parameters that are too high for smaller models and too low for larger ones. We attribute this failure to the implicit assumption that the spectral bias of an untrained INR remains static across different depths and widths. To address this, we propose using SECs to capture the frequency characteristics of images and models

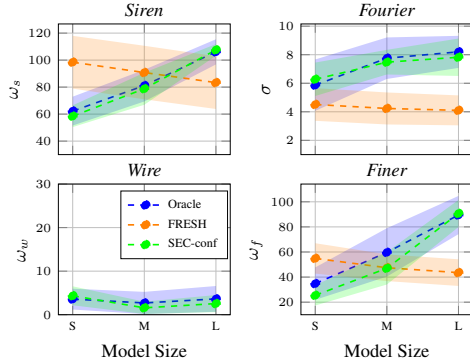


Figure 2: Mean embedding frequency parameter values selected using FreSh and SEC-conf on a benchmark of images sampled from the LIU4K-v2 dataset. Y-axis is scaled to reflect the range of tested parameter values. Optimal embedding frequency parameter values generally increase with model size (oracle). *Wire* is an exception, consistently requiring lower embedding frequency values to compensate for its naturally high spectral bias. While FreSh tends to select smaller values when network size increases, our method correctly tracks the oracle.

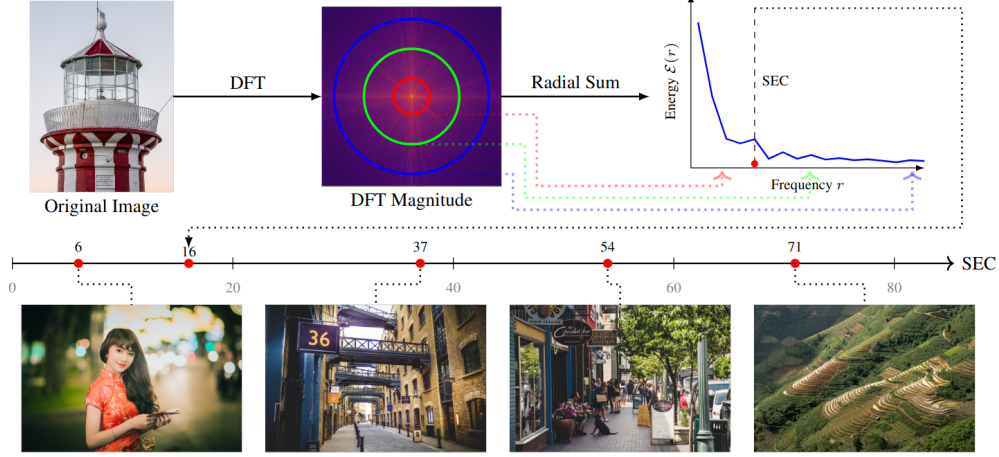


Figure 3: Visualization of the SEC calculation pipeline (top) and sample images with varying SEC values (bottom). To compute SEC, images are transformed via DFT and radial summation to obtain an energy spectrum, from which the centroid is computed. Our metric is correlated with visual complexity, as SEC increases images transition from smooth, blurry backgrounds to complex structures with high-frequency textures, such as dense foliage.

as a scalar value, which allows us to better understand spectral bias of various architectures and frequencies of target signals. Utilizing SEC, we create robust initialization strategies for embedding frequency parameters, align spectral bias between architectures and analyze image complexity.

3 Spectral energy centroid

Motivated by the observation that architectural changes can substantially alter the spectral bias of an INR, our goal is to obtain a representation of frequency that can be easily interpreted and used to improve our understanding of INR models. We first establish the foundations of spectral analysis and then introduce a metric that achieves this goal, Spectral Energy Centroid (SEC), and its applications.

3.1 Preliminaries

Discrete Fourier Transform (DFT) is used to analyze the frequency content of images. Let $A \in \mathbb{R}^{C \times N \times M}$ denote an image with C channels. The DFT of a channel c is:

$$\mathcal{F}_{u,v}(A_c) = \frac{1}{NM} \sum_{n=0}^{N-1} \sum_{m=0}^{M-1} A_{c,n,m} e^{-i2\pi(\frac{un}{N} + \frac{vm}{M})}, \quad (1)$$

where $u \in \{0, \dots, N-1\}$ and $v \in \{0, \dots, M-1\}$ are frequency indices. To facilitate further analysis and follow standard practice, we shift the frequency indices to be centered at zero. We define a shift operator that maps indices from a grid centered at $(0, 0)$ to the standard DFT grid:

$$\text{Shift}(u, v) = \left(u \bmod N, v \bmod M \right). \quad (2)$$

This allows us to consider frequencies on a grid $I = \{(u, v) \in \mathbb{Z}^2 : -\frac{N}{2} \leq u < \frac{N}{2}, -\frac{M}{2} \leq v < \frac{M}{2}\}$, where each point around $(0, 0)$ corresponds to low-frequency components of the DFT. Following FreSh, we consider $\text{Shift}(0, 0) = 0$, as the constant component of a signal can be easily modeled by an INR, yet it can be a major DFT component.

Energy spectrum. We define the **energy spectrum**, \mathcal{E} , as a vector representing how the energy of the original image is distributed across radial frequencies. Specifically, for an image A , the r -th element of \mathcal{E} captures the energy contained in frequencies with magnitude r :

$$\mathcal{E}(A, r) = \sum_{c=0}^{C-1} \sum_{\substack{(i,j) \in I \\ \lfloor \sqrt{i^2 + j^2} \rfloor = r}} |\mathcal{F}_{\text{Shift}(i,j)}(A_c)|^2. \quad (3)$$

This characterization leverages signal energy, defined as the squared magnitude of the Fourier coefficients. By Parseval’s theorem [11], the total energy is preserved between the spatial and frequency domains, which ensures that our spectral analysis faithfully reflects the information content of the original signal.

3.2 Spectral energy centroid

Energy centroid. While the energy spectrum describes the distribution of frequencies in detail, it is high-dimensional and difficult to use for direct comparison or optimization. To summarize the spectrum with a single statistic, we compute its mean weighted frequency. First, we normalize the energy spectrum to obtain a distribution $\tilde{\mathcal{E}}(A) = \frac{\mathcal{E}(A)}{\|\mathcal{E}(A)\|_1}$. The SEC of the image is then defined as the weighted average of frequencies under this normalized distribution (see visualization of this pipeline in fig. 3):

$$\text{SEC}(A) = \sum_{r=1}^R r \tilde{\mathcal{E}}(A, r), \quad (4)$$

where R is the highest radius that fits on an image. This quantity provides a robust measure of the central frequency with a clear interpretation - SEC represents the mean frequency weighted by signal power. We can compute SEC for: 1. target images to quantify their frequency content, 2. outputs of untrained models to approximate their spectral bias. For a model initialized with frequency parameter F , which outputs image A_{init} at initialization, we denote its SEC as $\text{SEC}(\text{Model}_F) = \text{SEC}(A_{\text{init}})$. We perform an ablation on design of SEC in section C.

Embedding configuration via SEC. The optimal frequency parameter depends on both the target image’s spectral properties and the model’s spectral bias, both of which can be measured by computing SEC for respective signals. However, the measurement of spectral bias is architecture dependent and can only be considered an approximation. To address this, we propose a data-driven approach. We assume that images with similar SEC scores share similar optimal configurations for a given architecture. We utilize a small calibration set of D examples $\{(A_i, F_i^*)\}_{i=1}^D$, where A_i is an image and F_i^* is the corresponding optimal embedding frequency parameter (e.g., found through grid search). Calibration images are randomly selected from the dataset. To configure an INR model for a new test image T , we set the relevant embedding frequency parameter to F_{i^*} by finding the nearest example from the calibration set:

$$i^* = \arg \min_i |\text{SEC}(T) - \text{SEC}(A_i)| \quad (5)$$

We refer to this approach as Spectral Energy Centroid-based Configuration (SEC-conf), and visualize the pipeline in fig. 4.

Frequency matching. Transferring optimal embedding frequency parameter configurations between different INR architectures has the potential to make model comparisons fairer by aligning their spectral biases, allowing to attribute any changes in observed performance strictly to architectural differences. Furthermore, it could simplify parameter selection for new models by leveraging well-configured models (e.g., *Finer*) to select the initial set of tested parameters. However, transferring frequency parameters between models is challenging as frequency parameters (e.g., ω_0 in *Siren*, σ in *Fourier*) have different interpretations and effects on the model. Consequently, hyperparameter values cannot be directly reused between them.

We hypothesize that while specific parameter values are not portable, the optimal spectral bias is at least partially transferable. Therefore, we propose Frequency Matching: a method to configure a

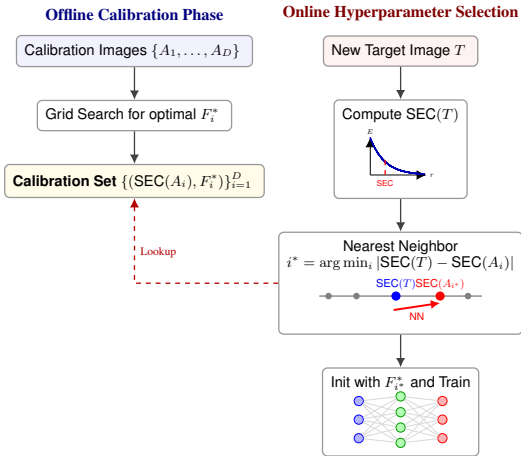


Figure 4: The SEC-Conf pipeline for INR hyperparameter selection. A calibration set is used to map Spectral Energy Centroids (SEC) to optimal frequency parameters. For a new target image, the optimal parameter is retrieved via nearest-neighbor matching in the centroid space.

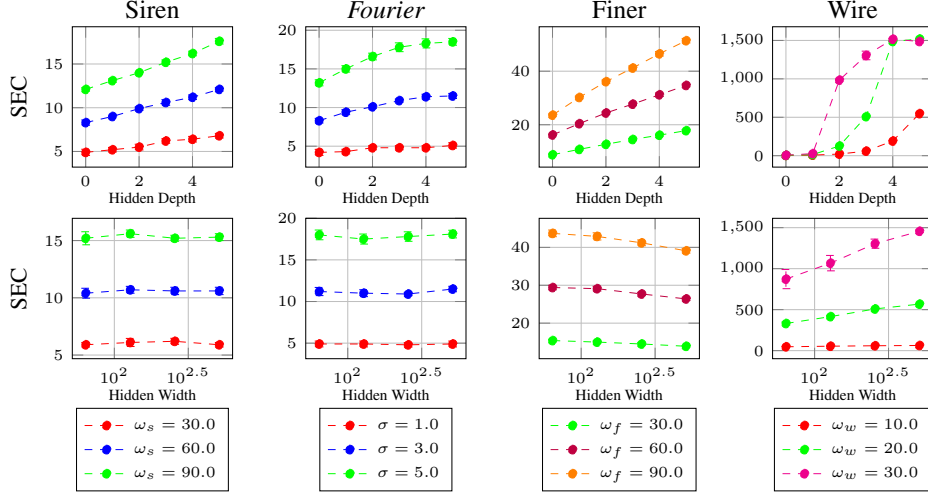


Figure 5: Relation between Energy centroid and model size. We measure SEC across various model sizes, by adjusting the number of layers or width of a 3-layer, 256-width MLP. We note that SEC can significantly increase with depth of the model, explaining why FreSh tends to incorrectly select lower embedding frequency parameter values for deeper models. However, SEC is not particularly affected by model width (except for *Wire*), suggesting that increasing width could be a safer strategy for scaling model capacity, as it preserves spectral properties. We note that *Wire* is a significant outlier, with extremely high frequencies present across almost all model sizes - we believe this high spectral bias explains why this architecture tends to perform poorly. SEC was measured 10 times at each frequency, and we plot both mean and 95% confidence interval.

target model by aligning its spectral bias with that of a reference model. Given a reference initialized model (e.g., a well-tuned architecture like *Finer*) with parameter F_{ref} , we denote the matched parameter value for a target model as $\text{Fit}_{F_{ref}}(F)$, where F is the parameter of the matched model (e.g., we will use ω_s when adjusting spectral bias of *Siren*). This value is obtained by finding the parameter F that minimizes the difference in spectral centroids:

$$\text{Fit}_{F_{ref}}(F) = \arg \min_F |\text{SEC}(\text{Model}_F) - \text{SEC}(\text{Ref}_{F_{ref}})|.$$

This approach allows us to translate configurations across disparate architectures without requiring expensive re-optimization.

4 Experiments

Energy centroid serves as a compact and interpretable summary of frequency content. In this section, we first analyze how model architecture influences SEC, providing insights into spectral bias. Building on this, we validate SEC’s practical utility by applying it to three distinct problems: guiding the selection of optimal embedding frequency parameters for new images, analyzing the relationship between image complexity and reconstruction quality, and aligning the frequency profiles of different architectures.

We conduct our experiments on a diverse benchmark of 100 images sampled from the LIU4K-v2 dataset [5], all down-sampled to a resolution of $2k \times 1.4k$. To evaluate our configuration strategies, we employ a random 10/90 calibration/test split, where 10 images are used to calibrate SEC-conf and the remaining 90 images serve as a held-out test set. We evaluate performance across three distinct model scales: small (S, 2×128), medium (M, 3×256), and large (L, 4×512). Our benchmark includes four representative INR architectures: *Siren*, *Wire*, *Fourier*, and *Finer*. For each architecture and model size, we perform an exhaustive grid search over their primary embedding frequency parameters: $\omega_s \in \{30, 40, \dots, 110\}$, $\omega_f \in \{10, 20, \dots, 100\}$, $\omega_w \in \{1, 5, 10, \dots, 30\}$, and $\sigma \in \{1, 2, \dots, 9\}$. All models are trained over 3 seeds for 15,000 optimization steps using the Adam optimizer [4] in PyTorch [12]. We describe compute resources used in section B.1.

4.1 Effects of architecture

We start by analyzing how the spectral bias of models, as approximated by SEC, varies with model architecture and size, with results presented in fig. 5. Our analysis reveals that SEC increases significantly with model depth across almost all architectures, confirming empirically theoretical results from previous work [23]. This likely explains the behavior of FreSh in fig. 2 - the method accounts for the depth-related increase in frequency by lowering the value of embedding frequency. This depth-induced increase in SEC shows that deeper models naturally favor higher frequencies and may require lower embedding parameters to achieve the same initial spectral bias as shallower counterparts. However, our results indicate that the increased capacity of deeper models allows them to better utilize high-frequency inputs. In our experiments, this capacity effect dominates, and deeper models consistently benefit from higher embedding frequencies.

In contrast to depth, model width has a negligible effect on spectral bias for most architectures. This suggests that scaling a model by width is more predictable than scaling by depth in terms of frequency characteristics. However, there are notable exceptions. For instance, the *Wire* architecture stands as an outlier, with a significantly higher SEC that shows a unique sensitivity to changes in width. We also observe that for *Finer*, increased width correlates with a decrease in SEC. This phenomenon is caused by the use of *Siren* weight initialization, which was tailored to sinusoidal (not variable-periodic) activations and assumes that inputs to each layer follow a standard normal distribution (see further discussion in section D). Such complex interactions between architecture and spectral bias underscore the necessity of a measurement-based approach like SEC for robust model configuration.

4.2 Prediction of embedding frequency parameters

As discussed in section 2, the optimal frequency parameter depends on both the target image’s spectral properties and the model’s capacity. Existing heuristics like FreSh account only for differences stemming from the target image and fail to account for architectural factors. In this section, we evaluate the performance of the SEC-conf-based configuration method (described in section 3), which leverages a small calibration set to predict optimal embedding frequency parameters.

Table 1 compares our method against FreSh and the standard baseline of default parameters. Our approach consistently outperforms the baseline and matches or exceeds the performance of FreSh, primarily because it accounts for architectural bias. This advantage is reflected in both the final reconstruction quality and the selection accuracy (see tables 1 and 2). We note that the absolute PSNR gap between SEC-conf and FreSh is bounded by the difference between the oracle and baseline configuration. In settings where the default is already near-optimal, no method - including ours - can show large gains. Where the gap is larger, SEC-conf reliably closes it, e.g. for large models.

Table 1: Comparison of reconstruction quality (PSNR) for models configured via our method versus baseline defaults and FreSh. We report mean performance and standard error computed across 3 seeds.

PSNR \uparrow	S	M	L
<i>Siren</i>	26.03 \pm 0.01	29.97 \pm 0.01	32.06 \pm 0.10
+BEST	26.64 \pm 0.01	31.31 \pm 0.01	34.60 \pm 0.03
+FRESH	26.45 \pm 0.02	31.21 \pm 0.01	34.07 \pm 0.07
+SEC-CONF	26.61 \pm 0.01	31.25 \pm 0.02	34.49 \pm 0.05
<i>Fourier</i>	24.72 \pm 0.04	27.68 \pm 0.11	29.01 \pm 0.03
+BEST	26.54 \pm 0.05	30.75 \pm 0.05	32.14 \pm 0.06
+FRESH	26.35 \pm 0.05	30.05 \pm 0.06	30.92 \pm 0.02
+SEC-CONF	26.35 \pm 0.07	30.45 \pm 0.14	31.74 \pm 0.08
<i>Finer</i>	27.26 \pm 0.02	31.86 \pm 0.01	34.23 \pm 0.01
+BEST	27.32 \pm 0.01	32.13 \pm 0.03	36.00 \pm 0.11
+FRESH	27.15 \pm 0.02	32.01 \pm 0.01	34.91 \pm 0.02
+SEC-CONF	27.21 \pm 0.02	31.99 \pm 0.01	35.81 \pm 0.07
<i>Wire</i>	24.39 \pm 0.02	27.70 \pm 0.04	28.67 \pm 0.08
+BEST	26.10 \pm 0.02	29.47 \pm 0.02	31.76 \pm 0.09
+FRESH	N/A	N/A	N/A
+SEC-CONF	26.07 \pm 0.01	29.43 \pm 0.03	31.58 \pm 0.17

Table 2: Accuracy of FreSh and SEC-conf in predicting the optimal frequency parameter. While SEC-conf’s accuracy is relatively low, just approximately tracking the oracle (see fig. 2) is enough for good performance.

ACCURACY \uparrow	L	M	S
<i>Siren</i> + FRESH	0.16	0.17	0.01
<i>Siren</i> + SEC-CONF	0.64	0.21	0.36
<i>Fourier</i> + FRESH	0.01	0.01	0.18
<i>Fourier</i> + SEC-CONF	0.32	0.20	0.21
<i>Finer</i> + FRESH	0.0	0.20	0.06
<i>Finer</i> + SEC-CONF	0.49	0.18	0.22
<i>Wire</i> + FRESH	N/A	N/A	N/A
<i>Wire</i> + SEC-CONF	0.47	0.47	0.57

For this reason, we also measure selection accuracy table 2, which better shows that SEC-conf demonstrates a substantially higher hit rate in identifying the optimal configuration as compared to the FreSh heuristic. The performance gain is particularly pronounced for larger models, where standard conservative defaults underestimate the required frequency and FreSh fails to account for increased model size (as discussed in section 2). While FreSh tends to suggest lower frequency parameters for larger models, our data-driven approach identifies that these models require higher frequency parameters. Additionally, we observe that while *Wire* possesses a significantly higher SEC than other architectures, this does not translate to superior performance. As shown in table 1, *Siren* consistently outperforms *Wire* across all model sizes, confirming that excessive high-frequency bias is detrimental. Additionally, we provide detailed training curves in section B.3, a cross-domain generalization study in section B.4 and additional metrics in section B.5.

Lastly, we acknowledge that while preparing the calibration dataset requires an upfront cost, results from our experiment can be reused for new images. We publish them together with a script to predict optimal embedding frequency parameter values for new target signals.³

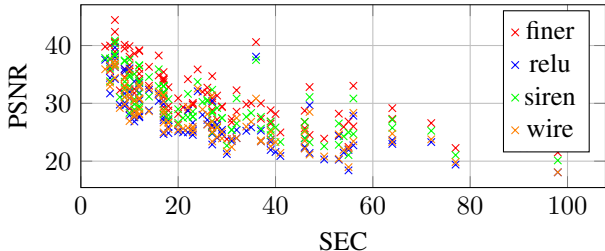


Figure 6: Relationship between SEC and reconstruction quality for Medium-sized models using default embedding frequency values. There is a strong correlation between SEC and PSNR, reflecting that SEC captures images complexity well.

Table 3: Spearman’s rank correlation between SEC and reconstruction quality (PSNR) for baseline models of size M.

CORR ↓	S	M	L
SIREN	-0.866	-0.822	-0.760
RELU	-0.839	-0.834	-0.845
FINER	-0.861	-0.796	-0.739
WIRE	-0.849	-0.843	-0.695

4.3 Spectral energy centroid and image complexity

Beyond hyperparameter selection, SEC serves as a robust proxy for image complexity, which we validate in this section by showing how increasing SEC correlates with a decreasing reconstruction quality across standard INR architectures. We present this relationship in fig. 6 for our 100-image dataset. In table 3 we observe a strongly negative Spearman’s rank correlation across all architectures. This confirms that images with higher spectral centroids - corresponding to finer details and textures - are harder to represent, resulting in lower PSNR values. While the correlation is significant, the spread in the data suggests that SEC alone does not fully dictate learnability. However, it remains a dominant factor. This relationship is additionally confirmed through images in fig. 3 and model outputs in section B.2. This analysis validates our score as a meaningful, scalar summary of signal difficulty, but also highlights the need for further investigation.

4.4 INR alignment via frequency matching

Directly comparing different INR architectures is challenging because each one starts with a different default frequency bias. To enable a fair comparison, we employ our frequency matching strategy to align spectral biases between architectures and isolate the effects of model architecture on performance. This ensures that performance gains are attributed to architectural design rather than superior tuning. We perform matching over the grid-search defined at the start of section 4. For robustness, the SEC values used for matching are calculated as the mean over 10 seeds. The results of this alignment are summarized in table 4, where we treat each architecture as a reference and match all other models to its initial spectral bias. See section B.6 for a discussion of specific parameter values used.

We first observe that standard *Siren* and *Fourier* models are typically initialized with similar, relatively low frequency biases. Consequently, matching between them results in no parameter changes and maintains their baseline performance gaps. However, when we align these conservative architectures

³<https://github.com/gmum/SEC>

with the *Finer* model, both *Siren* and *Fourier* see significant performance gains. This indicates that their default configurations are overly conservative, preventing them from capturing fine details. Notably, the large (L) *Siren* model, when matched to *Finer*, achieves performance parity with it. For smaller models, while matching improves performance, it does not fully close the gap, suggesting that *Finer* benefits from architectural advantages beyond its initial spectral bias.

As noted in section 4.2, the *Wire* architecture presents a unique challenge due to its high default SEC and we did not find a suitable matching of *Wire* to other architectures for medium and large models. When matching small *Wire* to other architectures, we select the minimum available frequency parameters - we note this improves the performance of *Wire*, which implies performance of this architecture could be further improved, if it was configured with a more conservative spectral bias, perhaps by avoiding the frequency increase at every layer. Conversely, matching other architectures to *Wire* often requires parameters beyond the searched grid.

Despite frequency matching offering only an approximate spectral-bias alignment, it can significantly impact the relative performance of diverse architectures. We hope it can serve researchers in finding good model configurations both in the context of testing old architectures, and developing new ones.

Table 4: Comparison of reconstruction quality for baseline models versus models with frequency parameters matched to a reference architecture. Note that for *Siren* and *Fourier*, the spectral profiles are similar, resulting in no parameter change. We exclude results for matching to *Wire* M and L models as their exceptionally high frequencies could not be matched within our hyperparameter grid. Results are averaged over 3 seeds, and we report standard error.

PSNR \uparrow	S	M	L
REF: <i>Finer</i>	27.09 ± 0.02	31.75 ± 0.02	34.14 ± 0.01
Fit $_{\omega_f=30}(\sigma)$	26.13 ± 0.09	29.95 ± 0.05	30.72 ± 0.03
Fit $_{\omega_f=30}(\omega_s)$	26.37 ± 0.02	31.13 ± 0.01	34.21 ± 0.05
Fit $_{\omega_f=30}(\omega_w)$	25.90 ± 0.02	—	—
REF: <i>Wire</i>	25.67 ± 0.01	28.84 ± 0.03	31.18 ± 0.12
Fit $_{\omega_w=10}(\omega_f)$	26.98 ± 0.02	—	—
Fit $_{\omega_w=10}(\sigma)$	26.17 ± 0.03	—	—
Fit $_{\omega_w=10}(\omega_s)$	26.12 ± 0.03	—	—
REF: <i>Siren</i>	25.86 ± 0.01	29.84 ± 0.01	31.97 ± 0.09
Fit $_{\omega_s=30}(\omega_f)$	26.39 ± 0.04	30.16 ± 0.02	31.81 ± 0.03
Fit $_{\omega_s=30}(\sigma)$	24.52 ± 0.05	27.53 ± 0.09	28.87 ± 0.03
Fit $_{\omega_s=30}(\omega_w)$	25.90 ± 0.02	—	—
REF: <i>Fourier</i>	24.52 ± 0.05	27.53 ± 0.09	28.87 ± 0.03
Fit $_{\sigma=1.0}(\omega_f)$	26.39 ± 0.04	30.16 ± 0.02	31.81 ± 0.03
Fit $_{\sigma=1.0}(\omega_s)$	25.86 ± 0.01	29.84 ± 0.01	31.97 ± 0.09
Fit $_{\sigma=1.0}(\omega_w)$	25.90 ± 0.02	—	—

5 Conclusion

In this work, we introduced SEC as a robust and interpretable metric for quantifying the frequency content of images and the spectral bias of INR models. Using this measure, we revealed that model architecture - specifically depth - significantly alters spectral bias, a factor overlooked by existing heuristics for hyperparameter configuration. While we demonstrated the practical utility of SEC through a data-driven hyperparameter configuration strategy and cross-architecture alignment, its primary value lies in offering a clearer lens for analyzing INR behavior. **By providing a scalar summary of spectral properties, SEC facilitates a deeper understanding of the relationship between signal complexity, model capacity, and reconstruction quality.** Our findings highlight the importance of architecture-aware frequency alignment and establish SEC as a valuable tool for future research.

Limitations

SEC is a one-dimensional scalar summary of the frequency spectrum. As such, signals with different spectral shapes may map to the same centroid value, and SEC cannot capture all nuances of frequency distributions. Additionally, SEC-conf relies on a calibration set obtained through offline grid search, unlike FreSh, which is a data-free heuristic operating on a single target image. This means the comparison between the two methods is not entirely apples-to-apples: SEC-conf has access to more information. This trade-off is a direct consequence of our goal of generality - the calibration set is what enables SEC to capture the relationship between spectral properties and model behavior across architectures and depths.

References

- [1] Hemanth Chandravamsi, Dhanush V. Shenoy, and Steven H. Frankel. Improving accuracy and efficiency of implicit neural representations: Making siren a winner, 2025.
- [2] Ali Gorji, Andisheh Amrollahi, and Andreas Krause. A scalable Walsh-Hadamard regularizer to overcome the low-degree spectral bias of neural networks. In Robin J. Evans and Ilya Shpitser, editors, *Proceedings of the Thirty-Ninth Conference on Uncertainty in Artificial Intelligence*, volume 216 of *Proceedings of Machine Learning Research*, pages 723–733. PMLR, 31 Jul–04 Aug 2023.
- [3] Adam Kania, Marko Mihajlovic, Sergey Prokudin, Jacek Tabor, and Przemysław Spurek. Fresh: Frequency shifting for accelerated neural representation learning. In *The Thirteenth International Conference on Learning Representations*, 2025.
- [4] Diederik P Kingma and Jimmy Ba. Adam: A method for stochastic optimization. *arXiv preprint arXiv:1412.6980*, 2014.
- [5] J. Liu, D. Liu, W. Yang, S. Xia, X. Zhang, and Y. Dai. A comprehensive benchmark for single image compression artifact reduction. *IEEE Transactions on Image Processing*, 29:7845–7860, 2020.
- [6] Zhen Liu, Hao Zhu, Qi Zhang, Jingde Fu, Weibing Deng, Zhan Ma, Yanwen Guo, and Xun Cao. Finer: Flexible spectral-bias tuning in implicit neural representation by variable-periodic activation functions. In *Proceedings of the IEEE/CVF Conference on Computer Vision and Pattern Recognition*, pages 2713–2722, 2024.
- [7] Marko Mihajlovic, Sergey Prokudin, Marc Pollefeys, and Siyu Tang. Resfields: Residual neural fields for spatiotemporal signals. In *The Twelfth International Conference on Learning Representations*, 2024.
- [8] Ben Mildenhall, Pratul P Srinivasan, Matthew Tancik, Jonathan T Barron, Ravi Ramamoorthi, and Ren Ng. Nerf: Representing scenes as neural radiance fields for view synthesis. *Communications of the ACM*, 65(1):99–106, 2021.
- [9] Tiago Novello, Diana Aldana, Andre Araujo, and Luiz Velho. Tuning the frequencies: Robust training for sinusoidal neural networks. In *Proceedings of the Computer Vision and Pattern Recognition Conference*, pages 3071–3080, 2025.
- [10] Vincent Ochs, Florentin Bieder, Sidaty el Hadramy, Paul Friedrich, Stephanie Taha-Mehlitz, Anas Taha, and Philippe C. Cattin. TabINR: An Implicit Neural Representation Framework for Tabular Data Imputation. *arXiv*, October 2025.
- [11] Alan V. Oppenheim, Alan S. Willsky, and S. Hamid Nawab. *Signals and Systems*. Prentice Hall, 2nd edition, 1997.
- [12] Adam Paszke, Sam Gross, Francisco Massa, Adam Lerer, James Bradbury, Gregory Chanan, Trevor Killeen, Zeming Lin, Natalia Gimelshein, Luca Antiga, et al. Pytorch: An imperative style, high-performance deep learning library. *Advances in neural information processing systems*, 32, 2019.
- [13] Nasim Rahaman, Aristide Baratin, Devansh Arpit, Felix Draxler, Min Lin, Fred Hamprecht, Yoshua Bengio, and Aaron Courville. On the spectral bias of neural networks. In *International conference on machine learning*, pages 5301–5310. PMLR, 2019.
- [14] Aravind Rajeswaran, Chelsea Finn, Sham M Kakade, and Sergey Levine. Meta-learning with implicit gradients. *Advances in neural information processing systems*, 32, 2019.
- [15] Basri Ronen, David Jacobs, Yoni Kasten, and Shira Kritchman. The convergence rate of neural networks for learned functions of different frequencies. *Advances in Neural Information Processing Systems*, 32, 2019.
- [16] Vishwanath Saragadam, Daniel LeJeune, Jasper Tan, Guha Balakrishnan, Ashok Veeraraghavan, and Richard G Baraniuk. Wire: Wavelet implicit neural representations. In *Proceedings of the IEEE/CVF Conference on Computer Vision and Pattern Recognition*, pages 18507–18516, 2023.
- [17] Vincent Sitzmann, Julien Martel, Alexander Bergman, David Lindell, and Gordon Wetzstein. Implicit neural representations with periodic activation functions. *Advances in neural information processing systems*, 33:7462–7473, 2020.
- [18] Matthew Tancik, Ben Mildenhall, Terrance Wang, Divi Schmidt, Pratul P Srinivasan, Jonathan T Barron, and Ren Ng. Learned initializations for optimizing coordinate-based neural representations. In *Proceedings of the IEEE/CVF Conference on Computer Vision and Pattern Recognition*, pages 2846–2855, 2021.

- [19] Matthew Tancik, Pratul Srinivasan, Ben Mildenhall, Sara Fridovich-Keil, Nithin Raghavan, Utkarsh Singhal, Ravi Ramamoorthi, Jonathan Barron, and Ren Ng. Fourier features let networks learn high frequency functions in low dimensional domains. *Advances in neural information processing systems*, 33:7537–7547, 2020.
- [20] Binxu Wang and Cengiz Pehlevan. An analytical theory of spectral bias in the learning dynamics of diffusion models. In *The Thirty-ninth Annual Conference on Neural Information Processing Systems, 2025*.
- [21] Yiheng Xie, Towaki Takikawa, Shunsuke Saito, Or Litany, Shiqin Yan, Numair Khan, Federico Tombari, James Tompkin, Vincent Sitzmann, and Srinath Sridhar. Neural fields in visual computing and beyond. In *Computer Graphics Forum*, volume 41, pages 641–676. Wiley Online Library, 2022.
- [22] Zhiqin John Xu. Understanding training and generalization in deep learning by fourier analysis. *arXiv preprint arXiv:1808.04295*, 2018.
- [23] Gizem Yüce, Guillermo Ortiz-Jimenez, Beril Besbinar, and Pascal Frossard. A structured dictionary perspective on implicit neural representations. In *Proc. IEEE/CVF Conference on Computer Vision and Pattern Recognition (CVPR 2022)*. June 2022.

A INR Architectures

This section provides the exact mathematical formulations for the coordinate embeddings and activations used in the architectures discussed in the main text.

Siren uses the following sinusoidal embedding:

$$\gamma_S(\mathbf{x}) = \sin(\omega_s \mathbf{W}\mathbf{x} + \mathbf{b}). \quad (6)$$

Fourier uses a fixed Fourier embedding:

$$\gamma_F(\mathbf{x}) = [\sin(2\pi \mathbf{W}\mathbf{x}), \cos(2\pi \mathbf{W}\mathbf{x})]. \quad (7)$$

Wire uses a complex Gabor wavelet activation:

$$\psi(x) = e^{j\omega_w x} e^{-|s_0 x|^2}. \quad (8)$$

Finer uses a variable-periodic activation:

$$\gamma_F(\mathbf{x}) = \sin\left(\omega_f(|\mathbf{W}\mathbf{x} + \mathbf{b}| + 1)(\mathbf{W}\mathbf{x} + \mathbf{b})\right). \quad (9)$$

B Additional results

B.1 Compute resources

We run our experiments using nodes of mixed GPUs, mainly with NVIDIA GeForce RTX 2070 and A100 40GB GPUs, with a single INR training taking up to 2 hours. In total, the grid search described in section 4 took around 5'400 hours. During initial exploration of SEC, we ran additional experiments that required a fraction of compute needed for the main grid search.

B.2 SEC at initialization

We visualize the relationship between the initialization hyperparameter ω_s and the Spectral Energy Centroid (SEC) for a *Siren* model in fig. 7. As ω_s increases, the SEC shifts toward higher values. This shift accurately reflects changes in the model’s spectral bias, where a larger SEC corresponds to finer, higher-frequency spatial features.

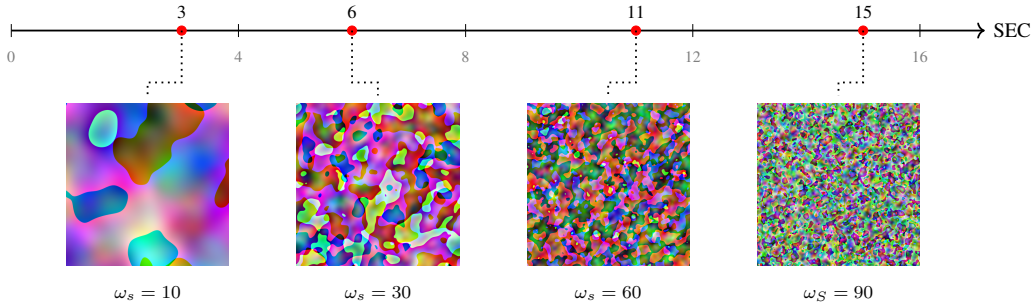


Figure 7: We visualize the effect of the initialization parameter ω_s on the SEC of a *Siren* model. Higher values of ω_s result in a monotonic increase in SEC, corresponding to the appearance of finer spatial details in the network’s initial output.

B.3 Training dynamics of SEC-conf

Figure 8 shows how mean PSNR evolves over the course of training for each configuration method. We train all models until convergence, as suboptimal frequency configurations can temporarily outperform better ones during early training stages. While this effect may not always be apparent when averaging over many images, it is visible in the small *Siren* setting, where FreSh briefly exceeds even the oracle configuration before falling behind.

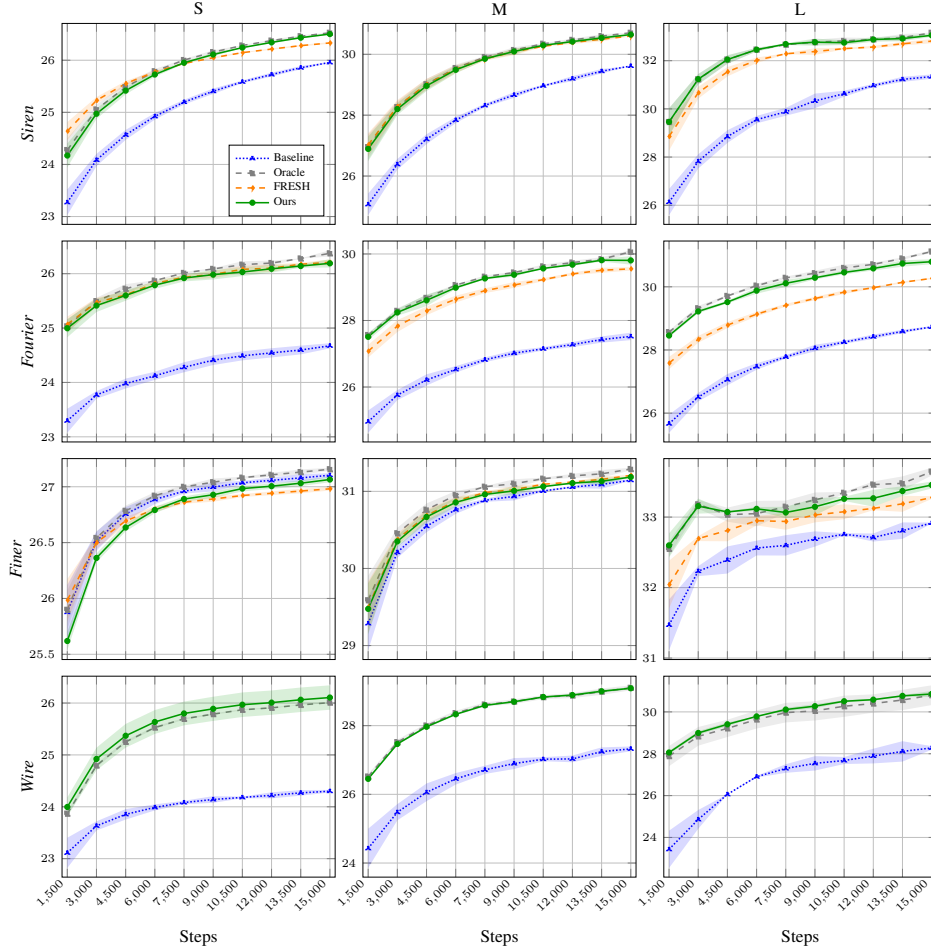


Figure 8: Mean PSNR over training steps for each configuration method across architectures and model sizes. Shaded areas indicate standard error.

Table 5: Comparison of reconstruction quality (SSIM) for models configured using various approaches.

SSIM \uparrow	S	M	L
<i>Siren</i>	0.680 \pm 0.0001	0.810 \pm 0.0005	0.870 \pm 0.0027
+BEST	0.693 \pm 0.0006	0.835 \pm 0.0002	0.900 \pm 0.0001
+FRESH	0.678 \pm 0.0011	0.828 \pm 0.0002	0.897 \pm 0.0005
+SEC-CONF	0.692 \pm 0.0006	0.832 \pm 0.0002	0.899 \pm 0.0004
<i>Fourier</i>	0.651 \pm 0.0016	0.746 \pm 0.0026	0.788 \pm 0.0009
+BEST	0.676 \pm 0.0012	0.819 \pm 0.0006	0.863 \pm 0.0012
+FRESH	0.678 \pm 0.0010	0.812 \pm 0.0010	0.841 \pm 0.0009
+SEC-CONF	0.669 \pm 0.0020	0.815 \pm 0.0021	0.858 \pm 0.0035
<i>Finer</i>	0.702 \pm 0.0003	0.846 \pm 0.0001	0.905 \pm 0.0002
+BEST	0.702 \pm 0.0003	0.843 \pm 0.0006	0.922 \pm 0.0008
+FRESH	0.684 \pm 0.0012	0.841 \pm 0.0003	0.913 \pm 0.0003
+SEC-CONF	0.702 \pm 0.0004	0.841 \pm 0.0002	0.920 \pm 0.0009
<i>Wire</i>	0.570 \pm 0.0017	0.695 \pm 0.0019	0.770 \pm 0.0040
+BEST	0.677 \pm 0.0008	0.787 \pm 0.0007	0.864 \pm 0.0014
+FRESH	0.000 \pm 0.0000	0.000 \pm 0.0000	0.000 \pm 0.0000
+SEC-CONF	0.674 \pm 0.0006	0.786 \pm 0.0008	0.862 \pm 0.0018

Table 6: Evaluation of SEC-conf on benchmark used by FreSh. Results for baselines and FreSh are taken from the FreSh paper, while results for SEC-conf were computed by us over 3 seeds. Overall, we observe an increase in performance, showing strong generalization capabilities of SEC-conf.

PSNR \uparrow	Average	Chest X-Ray	FFHQ-1024	FFHQ-wild	Kodak	Wiki Art
<i>Siren</i>	33.85 \pm 0.01	37.35 \pm >0.01	37.54 \pm 0.04	34.32 \pm 0.01	31.60 \pm 0.03	28.45 \pm 0.01
+FreSh	34.62 \pm 0.01	37.99 \pm 0.01	39.11 \pm 0.01	35.40 \pm 0.01	31.78 \pm 0.02	28.80 \pm 0.01
+SEC-conf	36.80 \pm 0.01	38.20 \pm 0.05	39.91 \pm 0.02	35.15 \pm 0.02	36.99 \pm 0.02	33.73 \pm 0.02
<i>Fourier</i>	32.12 \pm 0.01	36.96 \pm 0.03	35.01 \pm 0.04	32.65 \pm 0.01	28.84 \pm 0.04	27.15 \pm 0.01
+FreSh	33.45 \pm 0.02	37.77 \pm 0.04	36.81 \pm 0.06	34.62 \pm 0.01	30.06 \pm 0.01	28.01 \pm 0.02
+SEC-conf	35.09 \pm 0.11	38.20 \pm 0.12	37.66 \pm 0.11	34.40 \pm 0.04	33.51 \pm 0.21	31.65 \pm 0.16
<i>Finer</i>	35.11 \pm >0.01	38.63 \pm 0.02	40.45 \pm 0.01	36.48 \pm 0.02	31.40 \pm 0.02	28.57 \pm 0.01
+FreSh	35.03 \pm 0.01	38.51 \pm 0.04	40.31 \pm 0.07	36.48 \pm 0.01	31.31 \pm 0.03	28.54 \pm 0.01
+SEC-conf	37.63 \pm 0.02	39.10 \pm 0.07	41.54 \pm 0.02	36.09 \pm 0.01	37.35 \pm 0.01	34.04 \pm 0.02
<i>Wire</i>	33.54 \pm 0.02	37.96 \pm 0.02	38.13 \pm 0.04	35.04 \pm 0.01	28.95 \pm 0.06	27.62 \pm 0.01
+SEC-conf	33.48 \pm 0.07	36.81 \pm 0.02	36.52 \pm 0.02	33.03 \pm 0.01	31.58 \pm 0.01	29.48 \pm 0.38

B.4 Cross-domain generalization of SEC-conf

To further validate SEC-conf, we perform a cross-domain validation in table 6 on the benchmark used for FreSh [3]. We use SEC-conf with the same 10-image calibration dataset as used in section 4. We observe an increase in performance, showing strong generalization capabilities of SEC-conf. Particularly interesting is the particularly big performance gap on Kodak and Wiki Art datasets - those datasets are characterized by lower resolutions of images, which may indicate a connection between resolution and optimal embedding frequency selection strategy.

B.5 Additional reconstruction metrics

Table 5 presents results using SSIM (Structural Similarity Index) metric which captures perceptual quality more closely than PSNR. SEC-conf exceeds or matches the performance of FreSh also when considering this metric.

B.6 Network matching

Table 7 lists the specific frequency parameters selected by our matching algorithm ($\text{Fit}_{\text{ref}}(\cdot)$). Note that we limited our matching to parameters around the default values used for the respective models, which were included in our general grid search. While this restricted our search space for matching, it is not an inherent limitation of the method, and successful matching is achievable in all cases.

Additionally, we illustrate the outputs of matched models in fig. 9.

C Ablation Studies

To better understand which design choices are critical to performance, we perform a series of ablation experiments. We specifically focus on the formulation of the energy spectrum (see eq. (3)), where in the main method we consider the DC component as always equal to 0 ($\mathcal{E}(A, 0) = 0$), following the example of [3], as the DC component can have a significant effect on the signal while not making it harder nor easier to model. When the DC component is not zeroed, we label it as SEC-conf-DC. We also consider using DFT coefficients directly, as in FreSh, calculating the spectrum vector \mathcal{E} (note: values of this vector can no longer be interpreted as the power of the original signal) as:

$$\mathcal{E}_{\text{not power}}(A, r) = \sum_{c=0}^{C-1} \sum_{\substack{(i,j) \in I \\ \lfloor \sqrt{i^2+j^2} \rfloor = r}} |\mathcal{F}_{\text{Shift}(i,j)}(A_c)|. \quad (10)$$

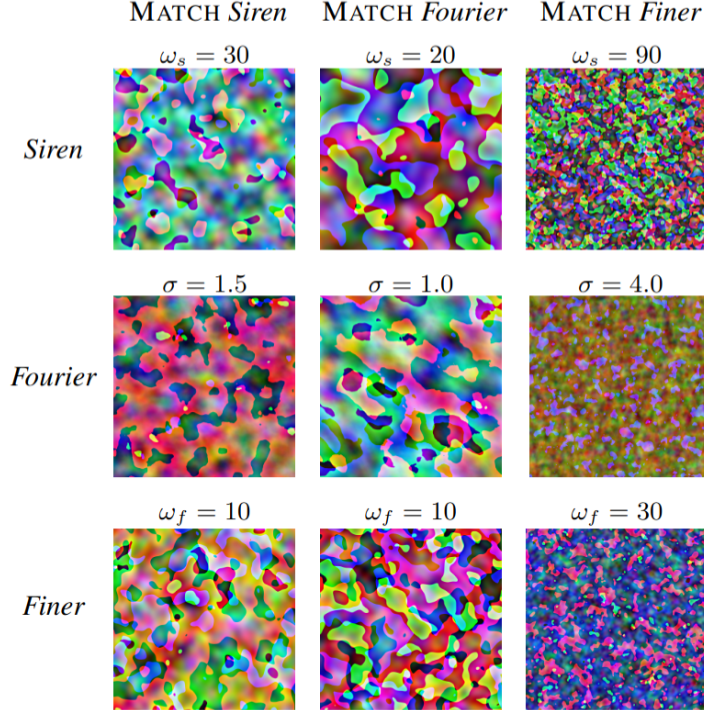


Figure 9: Network matching visualization: each row corresponds to a model architecture. The columns display: (1) Matched to *Siren*, (2) Matched to *Fourier*, (3) Matched to *Finer* (diagonal represents reference configurations). The parameter search for this visualization was denser than for the main results. The value of embedding frequency of the matched model is shown above each image. Observe that the outputs of unmatched models differ significantly but become similar after matching (images within a column are visually similar).

Additionally, we consider a modification to SEC, choosing a different statistic to convert $\mathcal{E}(A)$ into a scalar. Specifically, we consider the median instead of the mean. $\text{SEC}(A)$ is defined as the median of the energy spectrum. Formally, it is the smallest frequency f such that the cumulative energy up to f accounts for at least 50% of the total energy:

$$\text{SEC}(A) = \min \left\{ f : \sum_{r=0}^f \tilde{\mathcal{E}}(A, r) \geq 0.5 \right\}. \quad (11)$$

We present results from this ablation study in table 9 and fig. 10. First, we observe that the prediction of optimal frequency parameters and the resulting PSNR are not greatly affected by the specific choice of the statistic function used to calculate the centroid (see table 8). However, the correlation between SEC and the final reconstruction quality (PSNR) degrades when the energy spectrum is not squared, when the DC component is included, or when median is used instead of mean (see table 9). In the case of including the DC component, this degradation likely occurs because the high magnitude of the DC term compresses the range of SEC values, pushing them closer to zero and causing significant overlap between images with distinct frequency content, as visualized in fig. 10 (b).

D *Finer* Initialization

In this section, we investigate the effect of model width on the spectral properties of *Finer* to explain the behavior noted in section 4.1.

We start by noting that the *Siren* architecture [17] employs a carefully designed initialization scheme to control variance and limit the frequency increase within the network. Specifically, the pre-activation values (inputs to the nonlinearity) are expected to follow a standard normal distribution with unit

Table 7: Parameters selected during frequency matching. We report the selected parameter and the matching error (difference in SEC between reference and matched models). High errors (e.g., matching to *Wire*, or matching *Wire* to other models) indicate that the target architecture could not replicate the reference’s spectral bias within our search space.

	S		M		L	
	MATCHED PARAMETER	SEC ERROR	MATCHED PARAMETER	SEC ERROR	MATCHED PARAMETER	SEC ERROR
Fit $\omega_f=30(\omega_s)$	80.0	0.20	90.0	0.70	90.0	0.80
Fit $\omega_f=30(\sigma)$	4	0.70	4	0.20	4	0.10
Fit $\omega_f=30(\omega_w)$	10	7.40	10	45.10	10	190.50
Fit $\omega_w=10(\omega_f)$	50.0	0.40	100	14.10	100	157.20
Fit $\omega_w=10(\omega_s)$	110	3.00	110	41.20	110	186.40
Fit $\omega_w=10(\sigma)$	6	0.40	9	28.60	9	172.40
Fit $\omega_s=30(\omega_f)$	10	0.50	10	0.30	10	0.00
Fit $\omega_s=30(\sigma)$	1	1.00	1	1.40	1	1.20
Fit $\omega_s=30(\omega_w)$	10	14.50	10	53.40	10	199.80
Fit $\sigma=1.0(\omega_f)$	10	0.50	10	1.100	10	1.20
Fit $\sigma=1.0(\omega_s)$	30	1.00	30	1.40	30	1.20
Fit $\sigma=1.0(\omega_w)$	10	15.50	10	54.80	10	201.00

Table 8: Comparison of reconstruction quality (PSNR) for models configured via our method versus baseline defaults and FreSh.

PSNR \uparrow	S	M	L
<i>Siren</i>	26.03 \pm 0.01	29.97 \pm 0.01	32.06 \pm 0.10
+SEC-CONF	26.61 \pm 0.01	31.25 \pm 0.02	34.49 \pm 0.05
+SEC-CONF-MEDIAN	26.61 \pm 0.01	31.25 \pm 0.02	34.44 \pm 0.08
+SEC-CONF-NOT-POWER	26.60 \pm 0.01	31.23 \pm 0.01	34.54 \pm 0.02
+SEC-CONF-DC	26.62 \pm 0.01	31.25 \pm 0.02	34.52 \pm 0.04
<i>Fourier</i>	24.72 \pm 0.04	27.68 \pm 0.11	29.01 \pm 0.03
+SEC-CONF	26.35 \pm 0.07	30.45 \pm 0.14	31.74 \pm 0.08
+SEC-CONF-MEDIAN	26.21 \pm 0.01	30.52 \pm 0.15	31.65 \pm 0.01
+SEC-CONF-NOT-POWER	26.32 \pm 0.01	30.54 \pm 0.03	31.93 \pm 0.13
+SEC-CONF-DC	26.31 \pm 0.02	30.48 \pm 0.10	31.75 \pm 0.07
<i>Finer</i>	27.26 \pm 0.02	31.86 \pm 0.01	34.23 \pm 0.01
+SEC-CONF	27.21 \pm 0.02	31.99 \pm 0.01	35.81 \pm 0.07
+SEC-CONF-MEDIAN	27.23 \pm 0.02	31.99 \pm 0.01	35.76 \pm 0.05
+SEC-CONF-NOT-POWER	27.24 \pm 0.02	32.00 \pm 0.01	35.80 \pm 0.04
+SEC-CONF-DC	27.23 \pm 0.03	31.99 \pm 0.00	35.75 \pm 0.03
<i>Wire</i>	24.39 \pm 0.02	27.70 \pm 0.04	28.67 \pm 0.08
+SEC-CONF	26.07 \pm 0.01	29.43 \pm 0.03	31.58 \pm 0.17
+SEC-CONF-MEDIAN	26.06 \pm 0.02	29.44 \pm 0.03	31.64 \pm 0.11
+SEC-CONF-NOT-POWER	26.07 \pm 0.02	29.42 \pm 0.02	31.61 \pm 0.07
+SEC-CONF-DC	26.05 \pm 0.01	29.44 \pm 0.03	31.62 \pm 0.13

variance. Although *Finer* [6] adopts the same initialization strategy, it breaks the assumptions made by *Siren* by introducing an input-dependent scaling term $|\mathbf{W}\mathbf{x} + \mathbf{b}| + 1$:

$$\gamma_F(\mathbf{x}) = \sin\left(\omega_f(|\mathbf{W}\mathbf{x} + \mathbf{b}| + 1)(\mathbf{W}\mathbf{x} + \mathbf{b})\right). \quad (12)$$

We show the effect of this term on the intermediate outputs of *Finer* in fig. 11, where we plot the distributions of activations at various stages in *Finer* and *Siren* networks. We observe that the pre-sine activations of *Finer* exhibit higher variance than those of *Siren*, and this variance is width-dependent.

Table 9: Pearson correlation between SEC and reconstruction quality (PSNR). We compare (a) our default configuration (Mean) against variations: (b) including the DC component, (c) using non-squared spectrum, and (d) using Median instead of Mean.

(a) Default (Mean)				(b) With DC			
Corr ↓	S	M	L	S	M	L	
siren	-0.866	-0.822	-0.760	siren	-0.792	-0.760	-0.690
relu	-0.839	-0.834	-0.845	relu	-0.797	-0.771	-0.784
finer	-0.861	-0.796	-0.739	finer	-0.782	-0.741	-0.674
wire	-0.849	-0.843	-0.695	wire	-0.784	-0.764	-0.681

(c) Not Power				(d) Median			
	S	M	L	S	M	L	
siren	-0.132	-0.325	-0.432	siren	-0.547	-0.467	-0.404
relu	-0.033	-0.214	-0.301	relu	-0.574	-0.501	-0.503
finer	-0.166	-0.366	-0.463	finer	-0.538	-0.440	-0.389
wire	-0.031	-0.200	-0.292	wire	-0.578	-0.519	-0.420

Table 10: Accuracy of FreSh and SEC-conf in predicting the optimal frequency parameter.

PSNR ↑	L	M	S
<i>Siren</i> + SEC-CONF	0.64	0.21	0.36
+ SEC-CONF-MEDIAN	0.50	0.26	0.43
+SEC-CONF-NOT-POWER	0.84	0.29	0.46
+SEC-CONF-DC	0.77	0.23	0.41
<i>Fourier</i> + SEC-CONF	0.38	0.27	0.17
+SEC-CONF-NOT-POWER	0.54	0.33	0.18
+SEC-CONF-DC	0.27	0.19	0.16
<i>Finer</i> + SEC-CONF	0.44	0.19	0.54
+SEC-CONF-NOT-POWER	0.56	0.13	0.47
+SEC-CONF-DC	0.44	0.20	0.54
<i>Wire</i> + SEC-CONF	0.44	0.52	0.52
+SEC-CONF-NOT-POWER	0.62	0.57	0.43
+SEC-CONF-DC	0.54	0.54	0.54

Specifically, the variance of activations increases as the model width decreases. This increased variance in the inputs to the sine activation directly corresponds to higher frequencies, explaining the increase in SEC for smaller models observed in fig. 5. We believe this uncovers an interesting research direction for the *Finer* architecture, which would likely benefit from an initialization scheme tailored to its variable-periodic activations that would avoid the unexpected influence of width on spectral bias.

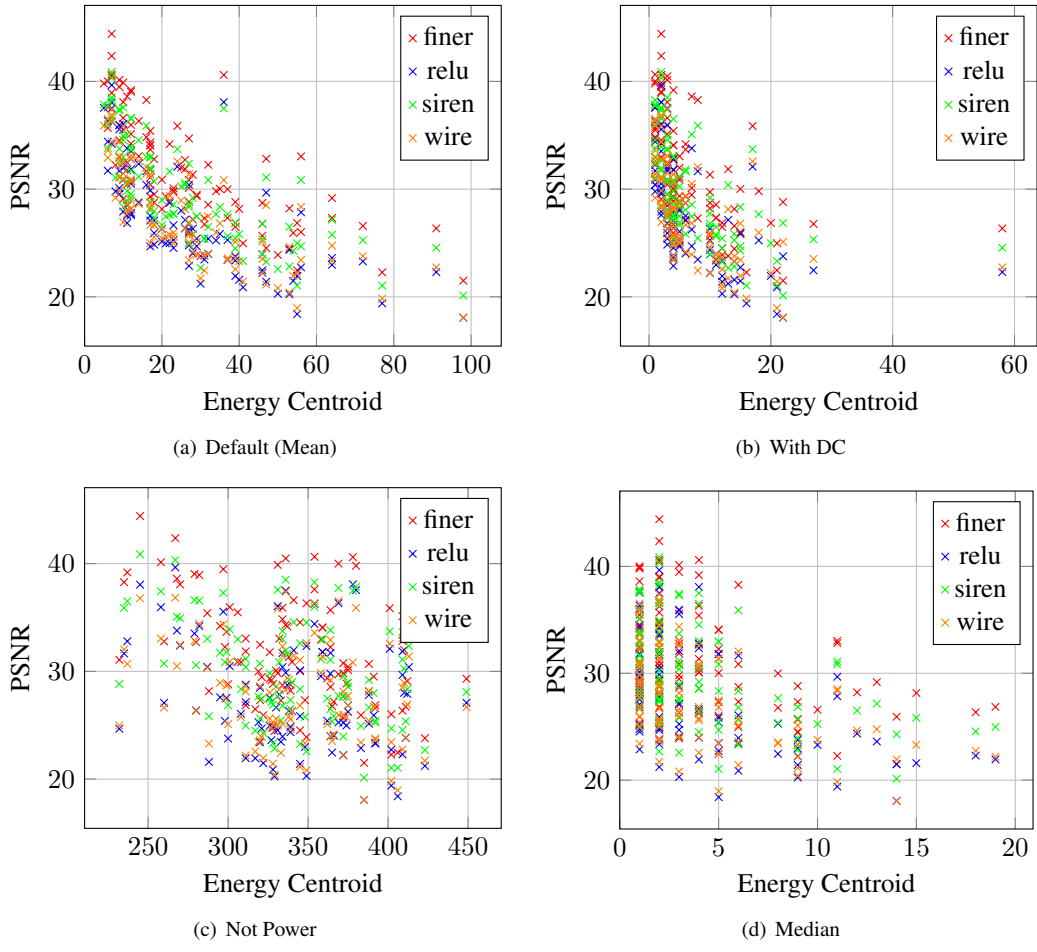


Figure 10: Relationship between SEC and reconstruction quality (PSNR) for Medium-sized models using default embedding frequency values. We compare (a) our default configuration (Mean) against variations: (b) including the DC component, (c) using non-squared spectrum, and (d) using Median instead of Mean.

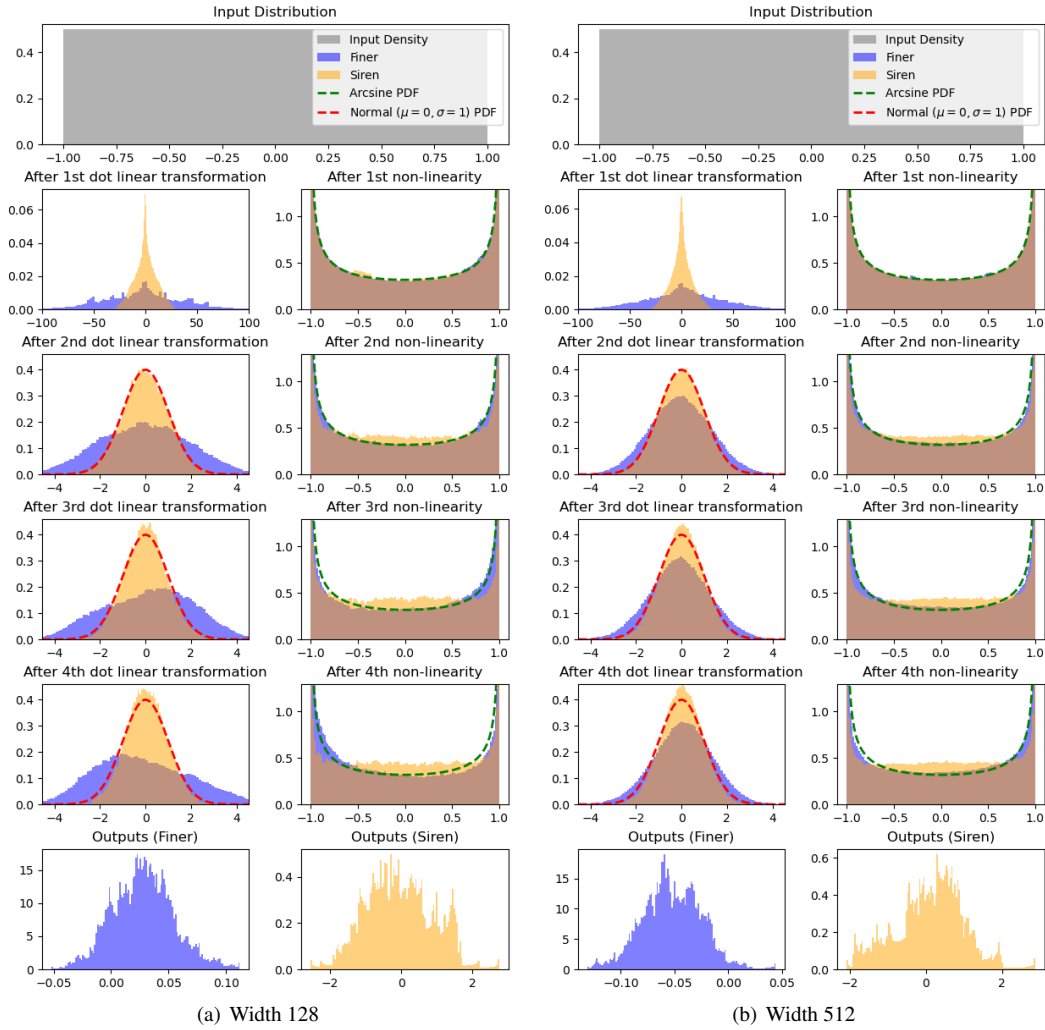


Figure 11: Distributions of pre- and post-activation (sine) values within *Finer* for different widths. Narrower models (left) exhibit higher variance in pre-activation values compared to wider models (right). This increased variance in the inputs to the sine activation directly corresponds to higher frequencies, resulting in higher SEC for narrower and deeper architectures.